Chloroplasts in plant cells show active glassy behavior under low-light conditions

Schramma, N.; Perugachi Israëls, C.; Jalaal, M.

DOI
10.1073/pnas.2216497120

Publication date
2023

Document Version
Final published version

Published in
Proceedings of the National Academy of Sciences of the United States of America

PNAS RESEARCH ARTICLE | APPLIED PHYSICAL SCIENCES

Chloroplasts in plant cells show active glassy behavior under low-light conditions

Nico Schramma[a], Cintia Perugachi Israëls[a], and Maziyar Jalaal[a,1]

Edited by Mehran Kardar, Massachusetts Institute of Technology, Cambridge, MA; received October 2, 2022; accepted December 10, 2022

Plants have developed intricate mechanisms to adapt to changing light conditions. Besides phototropism and heliotropism (differential growth toward light and diurnal motion with respect to sunlight, respectively), chloroplast motion acts as a fast mechanism to change the intracellular structure of leaf cells. While chloroplasts move toward the sides of the plant cell to avoid strong light, they accumulate and spread out into a layer on the bottom of the cell at low light to increase the light absorption efficiency. Although the motion of chloroplasts has been studied for over a century, the collective organelle motion leading to light-adapting self-organized structures remains elusive. Here, we study the active motion of chloroplasts under dim-light conditions, leading to an accumulation in a densely packed quasi-2D layer. We observe burst-like rearrangements and show that these dynamics resemble systems close to the glass transition by tracking individual chloroplasts. Furthermore, we provide a minimal mathematical model to uncover relevant system parameters controlling the stability of the dense configuration of chloroplasts. Our study suggests that the meta-stable caging close to the glass transition in the chloroplast monolayer serves a physiological relevance: Chloroplasts remain in a spread-out configuration to increase the light uptake but can easily fluidize when the activity is increased to efficiently rearrange the structure toward an avoidance state. Our research opens questions about the role that dynamical phase transitions could play in self-organized intracellular responses of plant cells toward environmental cues.

chloroplast | active glasses | active matter | organelle movement | glass transition

Significance

How can immobile plants adapt to ever-changing light conditions? Intracellular chloroplast motion is a fast adaptation mechanism which has been studied for more than 150 y. However, the role of collective motion of these organelles remained elusive. We show that dim-light–adapted chloroplasts exhibit glass-like features. We develop a mathematical model uncovering that chloroplast dynamics are close to a glass transition, which enables chloroplasts to quickly switch to a fluid-like phase for efficient avoidance motion. Besides their biological relevance, the light-dependent dynamical phases of the colloidal-like chloroplasts in *Elodea densa* constitute an intriguing model system to facilitate and broaden future research perspectives on dense active and living matter.

Plant sensing, consciousness, and movement have astonished scientists and philosophers since ancient times (1), from Plato—who in *Timaeus* (2) associated plants with a "soul" that lacks "judgment and intelligence" but shares "sensation, pleasure, pain, and desire"—to renaissance scientists like Porta, Bacon, and Hooke who wondered about the mechanism of plant movement, and to seminal work of Charles and Francis Darwin on plant behavior (3). It is now known that, despite generally being limited in their mobility, plants have evolved many movement mechanisms across both length and time scales to maintain optimal development and adapt to their environment (4, 5). Examples of these behavioral mechanisms are phototropism (response to light), gravitropism (response to gravity), and thigmotropism (response to touch). Such movements can occur on various time scales (4) and mostly on organismal length scales. However, the response to an environmental cue can also occur on a cellular scale. An example of such responses is the active reaction to light: on large scales, via phototropism, the plant grows and moves toward light (6). Meanwhile, on a small scale, chloroplasts can rearrange to optimize the photosynthesis and respiration processes (7–9). Hence, chloroplast motion enables plants to efficiently absorb light in order to generate metabolites as a product of photosynthesis while avoiding damage due to strong light. The light-induced movement of chloroplasts was first observed in the 19th century (10, 11). These organelles can change the direction of movement toward or away from light (12, 13) without turning (14, 15) but by photoreceptor-dependent redistribution of a chloroplast-specific membrane protein CHUP1 (16–18). This protein is essential for correct chloroplast positioning (19, 20) and acts as a nucleation factor (18) for chloroplast-specific short actin filaments (21, 22). Therefore, the CHUP1 distribution controls the binding affinity of short actin filaments which are polymerized and bundled by a plasma membrane–bound protein THRUMIN1 (23). If the CHUP1 distribution is asymmetric, the binding affinity of short actin filaments is biased and leads to a net propulsion force between the chloroplast and the plasma membrane of the cell (24). On the one hand, chloroplasts avoid strong light by fast escape movements (21, 25, 26), which leads to a decrease of potential photodamage (7, 27, 28). On the other hand, an accumulation response toward weak light sources (15, 29) leads to an increased absorption efficiency (9) as chloroplasts

Author affiliations: [a]Van der Waals-Zeeman Institute, Institute of Physics, University of Amsterdam, Amsterdam 1098XH, The Netherlands

Author contributions: N.S. and M.J. designed research; N.S., C.P.I., and M.J. performed research; N.S. analyzed data; and N.S. and M.J. wrote the paper.

The authors declare no competing interest.

This article is a PNAS Direct Submission.

[1]To whom correspondence may be addressed. Email: m.jalaal@uva.nl.

This article contains supporting information online at http://www.pnas.org/lookup/suppl/doi:10.1073/pnas.2216497120/-/DCSupplemental.

Published January 13, 2023.

self-organize into a dense layer on periclinal cell walls (30) (*SI Appendix*, Fig. S5*A*). This implies that chloroplast motion simultaneously maximizes photosynthetic performance while minimizing photodamage. Chloroplasts in various plants can achieve high surface fractions of around 70% upon the accumulation toward dim light (31, 32). Interestingly, higher numbers of smaller chloroplasts enhances mobility (33), while osmotic expansion of chloroplasts leads to effective inhibition of the light response (34). These observations point toward a dependence of the mobility of chloroplasts on their packing density and their individual activity. It has been shown in other biological systems that packing density and geometry impacts the fluidity and transport properties. Increased densities in confluent tissues can lead to a glass transition (35–37), arresting the cell motion and stabilizing the tissue in a solid-like state (38–40). Such rigidity transitions play a role in morphogenesis of zebrafish embryos (41), stabilize bronchial epithelium of the airway during development (42), and may be key to understand cancerous tissue (43). Moreover, even intracellular dynamics can exhibit features found in active granular liquids, as in the context of avalanching organelles for plant cell gravitropism (44), or feature glass-like transport properties in the cytoplasm in bacteria (45) or human cells (46). This indicates that active glassy dynamics occur across scales (47) and play a key role in understanding the structural changes and transport in and around cells.

In this study, we investigate the dynamics of chloroplast motion under dim-light conditions in the water plant *E. densa* (Fig. 1). We find that the dense, actively driven system shows dynamics similar to those of systems close to the glass transition, both in their overall statistics and individual particle dynamics. Despite the complexity of the system, we can construct a mathematical model that can reproduce the step-size statistics with experimental and physiological parameters. We use this model to test the stability of the state close to the glass transition and show that the chloroplast motion can exhibit more liquid-like dynamics when the activity slightly increases. Our observations suggest that chloroplasts naturally organize close to a critical point in order to reach a large area coverage. Consequently, chloroplasts increase photosynthetic efficiency while maintaining the ability to quickly respond to unfavorable light conditions by actively fluidizing the configuration for efficient avoidance movement.

Light-Dependent Dynamical Phases of Chloroplasts

We investigate the motion of 728 chloroplasts 20 min before and after the transition from dim red light to bright white light conditions (*Materials and Methods* and Movie S1). Before the onset of the light stimulus, the dim-light–adapted chloroplasts are found to be positioned in a single layer at the bottom of the cell as confirmed by confocal laser scanning microscopy (Fig. 1*C*). Within the first 20 min chloroplasts do not move far from their initial position, as indicated by the maximal traveling distance in Fig. 2*A*. As the light conditions are changed, the chloroplasts rapidly leave their local position and move far distances, corresponding to multiple chloroplast diameters.

Simultaneously, the instantaneous speed of the chloroplasts increases significantly by an order of magnitude (Fig. 2*B*). We further observe that chloroplasts also escape from a two-dimensional to a three-dimensional configuration. To further study the difference in the motion in both regimes, we consider the mean squared displacement (MSD) (Fig. 2*C*). Notably, the

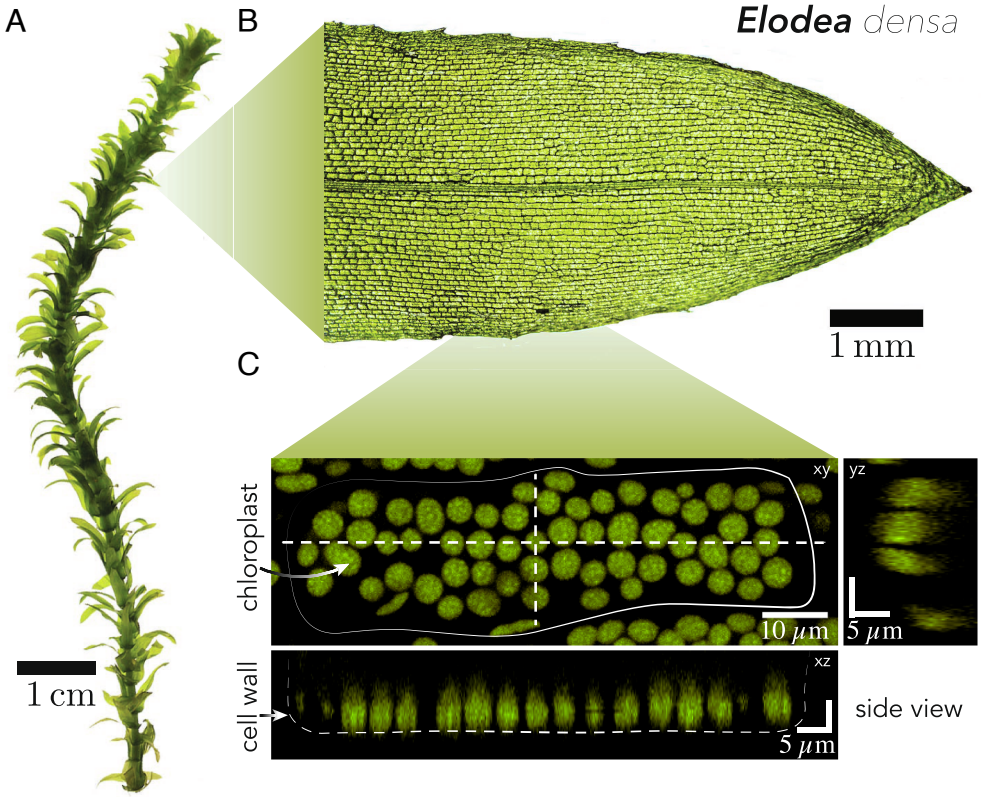

Fig. 1. (*A*) *Elodea densa* water plant as cultured under controlled environmental conditions. (*B*) Leaves are detached from the plants. (*C*) Laser scanning confocal microscopy image of chloroplasts inside a single epidermal cell. Chloroplasts (in green) are spread out in a single layer under dim-light conditions as indicated by the side view along the dotted line representing the position of the cell wall.

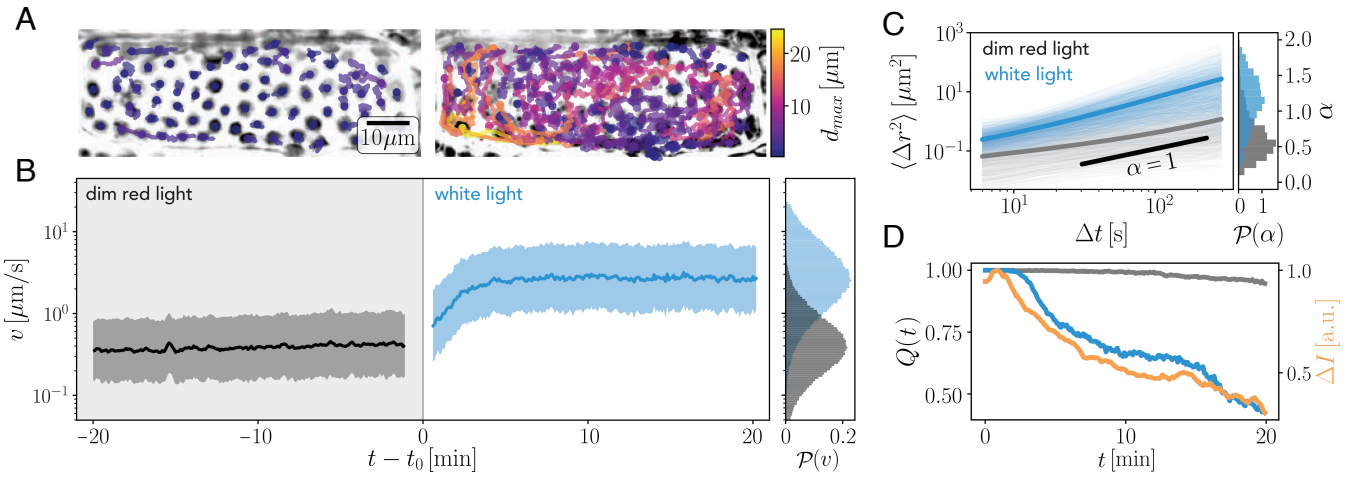

Fig. 2. Light adaptation of chloroplasts. (*A*) Trajectories of chloroplasts in a single cell for 20 min before (*Left*) and after (*Right*) the onset of bright light. Color bar: maximal distance from the initial position. (*B*) The speed v changes by one order of magnitude before (gray) and after (blue) the light stimulus at time t_0. The gap is due to the manual change of filter, light intensity, and exposure time which lasted 3 min. *Right*: Histograms of the speed distributions for all trajectories and all times. (*C*) Mean squared displacement acts as an indicator of enhanced activity. White light (blue line) triggers mainly diffusive to superdiffusive motion at time scales around $\Delta t = 10 - 100$ s, while dim-light–adapted chloroplasts (gray) are mainly subdiffusive. The histogram displays the probability density of anomalous diffusion exponents α. (*D*) Self-overlap function of the dim-light–adapted state (gray) and the light-adapting chloroplasts (blue). The orange line indicates the relative change in average intensity in the raw microscopy data indicating decreasing light absorption.

dynamics do not only show a higher baseline according to an anomalous diffusion coefficient D but also a change of scaling exponent α from a mostly subdiffusive ($\alpha < 1$) to a superdiffusive ($\alpha > 1$) scaling, when fitted with a powerlaw $MSD(\Delta t) = 4D\Delta t^{\alpha}$ at times $\Delta t = 10 - 100$ s. We further quantify the motion of the chloroplasts by defining a self-overlap function $Q(t) = \langle H(r_{th} - r(t)) \rangle$, with $H(x)$ being a Heaviside function $H(x) = 1$ if $x \geq 0$ and $H(x) = 0$ else and $\langle \dots \rangle$ being the average over all particles. This function represents the temporal evolution of the fraction of chloroplasts which move not further than $r_{th} = 5\,\mu$m (about one chloroplast diameter; *SI Appendix*, Fig. S1*G*) away from their initial position. The slow relaxation of this function at dim-light conditions is due to smaller rearrangements in the dim-light–adapted phase. Upon initiation of the white light stimulus, however, Q drastically decreases, indicating the fast rearrangements (Fig. 2*D*). This strong-light adaptation happens within a short period of 40 min and results in a cellular structure, which increases the transmittance of the leaf, and hence decreases overall light absorption (Movie S1). We further quantified this transmittance by analyzing the raw intensity values from the microscope time series. We took the pixel intensity average $I(t)$ and calculated $\Delta I(t) = (I_{max} - I(t))/(I_{max} - I_{min})$, the relative difference to the maximal transmitted light intensity normalized by the difference between the minimal intensity after the onset of light and maximal transmitted intensity, when chloroplasts are aggregated (Fig. 2*D*). This decrease in absorbance will cause smaller photodamage, as has been studied previously in a variety of plants (7, 26–28).

This transition from a dim- to a strong-light–adapted state, is therefore of high physiological relevance for the plant. But how do chloroplasts behave under dim-light before the onset of the transition? How stable is the densely packed two-dimensional configuration? These questions we aim to answer in the following.

Glassy Features of Chloroplast Motion Under Dim Light

We track the positions of 1,529 chloroplasts under dim light and constant environmental conditions and segment their morphological features (*Materials and Methods*). In dim-light, chloroplasts decrease their mobility (13) and settle onto the periclinal walls in a single layer (Fig. 1*C* and Movies S1–S3). Chloroplast motion is based on the polymerization of specialized short actin filaments in the space between the chloroplasts' outer membrane and the cell membrane (21, 22) (*SI Appendix*, Fig. S5). Therefore, membrane anchoring is essential for the propulsion of the organelle (48), which only allows for essentially two-dimensional motion. Under dim-light conditions, the binding probability of actin on the chloroplast is not biased in any direction, which will cause zero net motion. However, fluctuations, driven by random actin binding events, constitute a nonthermal random motion.

Chloroplasts appear as flat circular disks, with an average aspect ratio $AR = 1.2$ and mean radius $R = 2.29 \pm 0.29\,\mu$m (mean ± s.d.) corresponding to a polydispersity of about 12.6% (*SI Appendix*, Fig. S1 *G* and *J*). We measure a two-dimensional average packing fraction of approximately 73%, which is consistent with measurements in land plants (31, 32). This suggests that chloroplast motion may depend on their close-by neighbors.

Because they can move in all directions without rotating (15), the orientation of the chloroplast is uncoupled from the migration direction. Consequently, an analysis of the two-dimensional center-of-mass trajectories alone is sufficient to elucidate underlying stochastic processes. The mean-squared displacement (Fig. 3*A*) reveals a broad spectrum of power law exponents α at small time scales ($\Delta t = 10 - 100$ s), ranging from subdiffusive to superdiffusive trajectories (histogram in Fig. 3*A*). At long time scales of $\Delta t \gtrsim 5$ min, the MSD approaches overall diffusive scaling ($\alpha = 1$), with approximately exponentially distributed diffusion coefficients (Fig. 3*D*) and average diffusion coefficient $D \approx 8 \times 10^{-4}\,\mu$m^2/s. This diffusion coefficient is based on actin binding and polymerization (21), rather than thermal diffusion. To test this, we inhibited the active motion by a strong blue light shock, which drastically decreases the agitation, leaving the thermal diffusion undetectable (*SI Appendix*, Fig. S2 and Movie S5).

The velocity autocorrelation reveals that the velocity v of chloroplast motion decorrelates within several seconds (Fig. 3*B*),

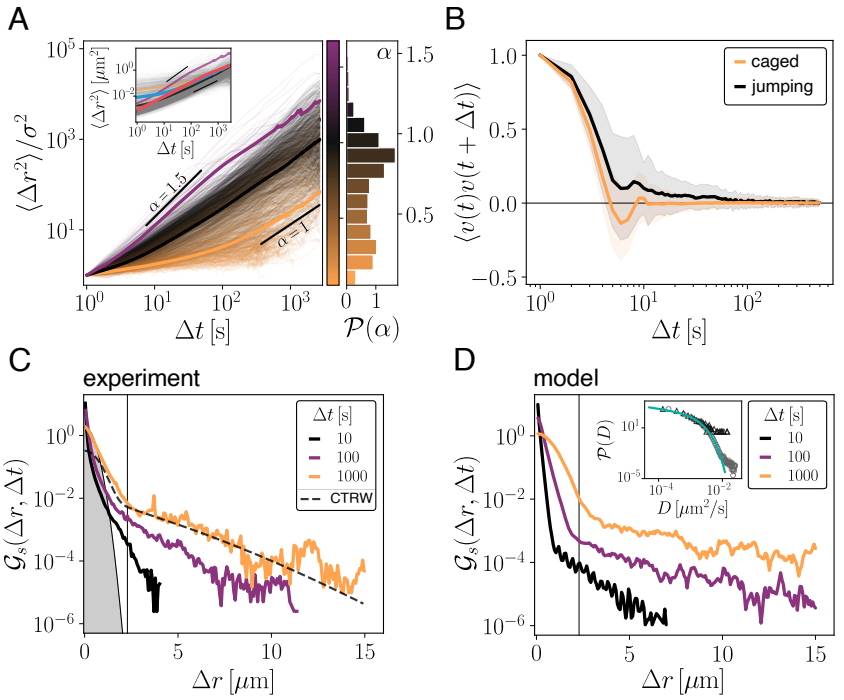

Fig. 3. Trajectory analysis reveals subdiffusive to superdiffusive transport and local trapping. (*A*) MSD of all trajectories relative to a minimal displacement scale $\sigma = MSD(\Delta t = 1\,\mathrm{s})$. Colormap represents the power-law scaling exponent α fitted on short time scales below 100 s. The exponent is widely distributed but peaks around a diffusive scaling regime ($\bar{\alpha} \approx 0.9$). While many trajectories show subdiffusive scaling laws at small times, a few trajectories exhibit superdiffusive scaling. Thick lines: Ensemble averages over superdiffusive trajectories $\alpha \geq 1.1$ (purple), diffusive trajectories $0.5 < \alpha < 1.1$ (black), and strongly subdiffusive trajectories $\alpha \leq 0.5$ (orange). Notably on large time scales, all regimes approach a diffusive scaling. Inset: MSD with units, most trajectories reach 1-micrometer displacement after long time ($t > 100$ s) only. Thick lines compare the ensemble average of all trajectories (blue line) to the ensemble-averaged MSD of simulations (red line). Purple, black, and orange lines correspond to ensemble averages in the main panel. Histogram: Bimodal distribution of scaling exponents $\boldsymbol{\mathcal{P}}(\alpha)$. (*B*) Velocity autocorrelation functions (VACF) of trapped (orange) and jumping (black) chloroplasts. Some jumping chloroplast exhibit pronounced temporal correlation, which shifts the VACF to higher values. Anticorrelation as a sign of fast reorientations is less pronounced in jumping chloroplasts, indicating a directed motion. (*C* and *D*) Self part of the radial van Hove function at different lag-times for experiments (*C*) and model (*D*) reveals non-Gaussian displacements on short lag-times (compare with the gray area, representing a Gaussian function). For larger lag-times, the distributions are approaching a Gaussian at small displacements, hence the comparison with a continuous time random walk (CTRW) model (49) (dashed line in *C*) improves. The proposed model (*D*) accounts for the exponential tails, starting at a critical displacement (vertical line), and the exponential-to-Gaussian crossover at small displacements. *Inset*: Diffusion coefficients of experiments (triangles) and simulation (circles) can be well described by a corrected exponential distribution (solid line).

indicating a persistent motion on these time scales. Together with the MSD scaling exponents, the velocity autocorrelation demonstrates a clear picture of the individual dynamics of chloroplasts: They are driven by a stochastic process which has a back-reflection effect, as suggested by the anticorrelation of the velocity after a few seconds (Fig. 3*B*). A few trajectories show slightly more persistent motion and larger scaling exponents indicating coordinated movement of actively driven chloroplasts.

To further investigate the nature of the stochastic process constituting the motion of densely packed chloroplasts, we study the self-part of the van Hove function (step-size distribution) $\mathcal{G}_s(\Delta r, \Delta t)$ (Fig. 3*C*) at various delay times $\Delta t = 10, 100, 1{,}000$ s. Strikingly, the van Hove function deviates from a Gaussian function at small and large displacements in two distinct manners. First, small displacements are governed by a transition from a non-Gaussian to a Gaussian step-size distribution for increasing delay times. This feature is commonly found in the dynamics of (fractional) Brownian, non-Gaussian diffusive motion and has been observed in organelle and RNA transport (50, 51). Second, the chloroplast step-size distribution exhibits an exponential tail at all time scales. The transition toward the exponential tail happens around $\Delta r \approx 2.3\,\mu$m, corresponding to one average chloroplast radius $R \approx 2.29\,\mu$m (*SI Appendix*, Fig. S1*G*). This displacement is more than five times as large as the inter-chloroplast distance $l \approx 0.42\,\mu$m, which is calculated via the difference of average chloroplast diameter and nearest neighbor distance (52) (*SI Appendix*, Fig. S1 *G* and *F*). Hence, small displacements $\Delta r < l$ correspond to free motion until a chloroplast reaches l. Larger displacements $l \leq \Delta r < 2.3\,\mu$m are likely connected to the interaction of multiple chloroplasts, while displacements exceeding 2.3 μm show a sudden transition toward an exponential step-size distribution. Such an exponential tail has been previously observed in other systems on various scales, such as the bacterial cytoplasm (45), particle transport in human cells (46), motion of cells in confluent tissues (35), and nonactive systems like supercooled liquids (53) and colloidal glasses (54). Using a continuous-time random walk (CTRW) model, it was shown that exponential tails of the van Hove function display a universal feature of particle motion close to the glass transition (49, 55), which can be fitted to our experimental results (dashed line in Fig. 3*C*). However, this model does not fully account for the non-Gaussian center of the observed distribution, as we will discuss in more detail later.

With a high packing fraction of $\phi \approx 73\,\%$ (*Materials and Methods*), the amorphous chloroplast monolayer bears a noticeable structural resemblance with dense colloidal systems, which may explain the key features of chloroplast motion. The direct study of individual trajectories in colloidal glasses has led to the conclusion that the stretched exponential step-size distribution arises as a result of heterogeneous dynamics of slow and fast particles (54). This heterogeneity was found in active

systems and also constitutes a hallmark for glasses (47). Hence, our observation of the exponentially tailed step-size distribution indicates the existence of dynamical heterogeneity underlying chloroplast motion.

Dynamic Heterogeneity Due to the Coexistence of Locally Entrapped and Rearranging Chloroplasts

The aforementioned hypothesis requires analysis of individual chloroplast trajectories. We find qualitatively different trajectories. While many chloroplasts remain caged by their neighbors (slow particles), a small fraction (88 of 1,529) can escape their local confinement and move for longer distances until they get trapped again as a jump-like motion (fast particles) (Fig. 4 *A* and *E*). The dynamic heterogeneity is studied by disentangling the fast and slow dynamics of the system, based on the chloroplasts maximal displacement d_{max} during the experimental time (Fig. 4*E*) (54, 56) and their maximal speeds (*Materials and Methods*).

We uncover large regions of trapped particles and smaller regions of more mobile chloroplasts (Fig. 4*A* and *SI Appendix*, Fig. S1*A*) by marking trajectories by their total displacement from their initial position. Fast chloroplasts rearrange within a short period of time and arrest the dynamics afterward. The intermittent bursts of chloroplast relocations can be detected in the tails of the speed distribution (Fig. 4*B*), as represented by the 95th percentile, while the average speed does not exhibit strong changes. This confirms that rearrangements are connected to exceptionally high speeds of chloroplast motion, which transiently occur in a small fraction of all chloroplasts in a cell. Besides the spatial colocalization of chloroplast relocations, we find that their motion can be temporally correlated and follows a string-like profile. Individual chloroplasts can break out of their local cage and push their neighbors with them (Fig. 4 *C* and *D* and *SI Appendix*, Fig. S1*A*). Additionally, fast chloroplasts have longer velocity autocorrelation times, suggesting an increase in the persistent motion, while slow particles oppose their motion on smaller time scales (Fig. 3*B*). The movement of all rearranging chloroplasts follows a similar scheme: a sudden chloroplast displacement at elevated velocities plateaus at a distance of only a few chloroplast diameters (Fig. 4 *E*, *Inset*). This suggests that they are locally entrapped again.

Differences in the dynamics, however, cannot be simply ascribed to structural differences as suggested by the absence of strong correlations between structural features like the particle radius, average nearest neighbor distance, and aspect ratio and dynamic features like the maximal traveling distances and maximal speeds of individual trajectories (*SI Appendix*, Fig. S1 *A*–*E*). Similar sudden and hardly predictable rearrangements have been found in simulations of active Ornstein–Uhlenbeck particles (57), sheared granular media (58), and in epithelial tissues (35). Interestingly, the string-like cooperative motion of particles in a close-to-glassy state was observed in supercooled liquids (59, 60), simulations of Lennard-Jones mixtures (61) and granular beads (62).

The striking similarity to many systems close to the glass transition implies that chloroplast motion in this dense single-layered configuration obeys similar physical constraints and mechanisms. In the following, we will build a mathematical formulation based on physiological parameters that models the coexistence of trapped particles and regions of higher mobility in the chloroplast dynamics in the two-dimensional (2D) configuration. This approach allows us to study the effect of activity and crowding on chloroplast dynamics. Our goal is to infer the stability around the critical state of the chloroplast monolayer.

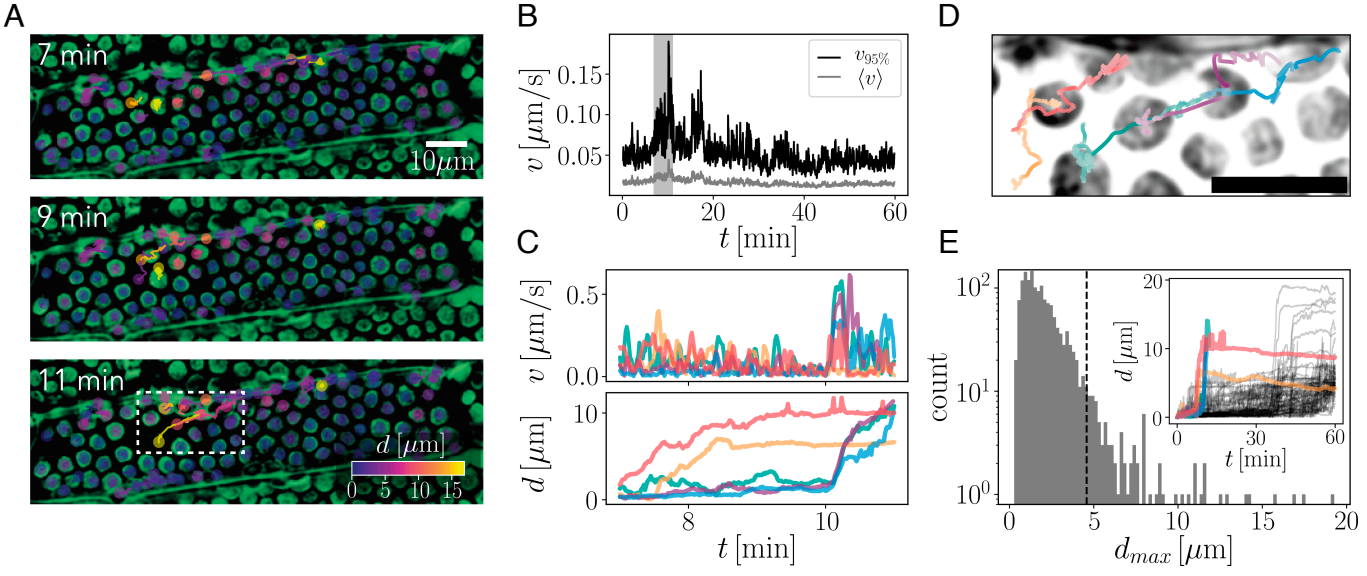

Fig. 4. Intermittent rearrangements of chloroplasts. (*A*) Time series of chloroplast motion during a bursting event. Trajectories are color-coded by their final distance *d*. While most chloroplasts remain at their initial location, a small region shows enhanced activity (white box). (*B*) Time series of average velocity (gray) and the 95th percentile velocity (black) of the cell in (*A*). The gray region around the peak corresponds to the time series in (*A*) and (*C*). The large increase of the 95th percentile indicates that the single event is an extreme of the velocity distribution. (*C*) Velocity and distance *d* from the initial position for trajectories which undergo strong rearrangement (*A*, white box). Correlated motion of the sudden relocation becomes apparent. Colors for comparison of trajectories in (*C*) and (*D*). (*D*) Close-up of trajectories in (*A*), white box. Chloroplasts show random trapped motion, followed by transient collective motion, and subsequent fluctuations. (Scale bar, 10 μm.) Higher color saturation along the trajectories indicates enhanced speed. (*E*) Histogram of maximal displacements with the threshold value (dashed line, *Materials and Methods*). *Inset*: Distance from the initial position for all chloroplasts exceeding the distance threshold showing similar pattern: sudden rearrangements and subsequent plateau at approximately discrete positions of a few chloroplast diameters. Trajectories from (*C*) and (*D*) are marked in respective colors.

A Threshold-Based Jump Diffusion Model Reveals that the Dim-Light–Adapted Chloroplast Monolayer Is Close to a Glass Transition

We propose a stochastic model of chloroplasts to elucidate the impact of critical length-scales and active diffusion of the system. In this model, discrete jumps are triggered by a threshold-based mechanism (Fig. 5*A*). We consider a particle in a harmonic potential $V(x) = -\frac{k}{2}x^2$ that can undertake a jump of finite velocity v upon exceeding a critical distance x_c from the potential minimum position $a(t)$. This leads us to a Langevin equation:

$$\dot{x} = \begin{cases} -\frac{x}{\theta} + \sqrt{2D(t)}\xi(t), & |x - a(t)| < x_c \\ -\frac{x_c}{\theta} \pm v + \sqrt{2D(t)}\xi(t), & |x - a(t)| \geq x_c, \end{cases} \quad [1]$$

where $\xi(t)$ is a Gaussian white noise $\langle \xi \rangle = 0$, $\langle \xi(t)\xi(t') \rangle = \delta(t - t')$. The effective spring constant k represents confinement by actin-mediated anchoring (48) and the neighboring particles (63, 64). Together with a damping prefactor γ, it defines a correlation time $\theta = \frac{\gamma}{k}$. Our analysis allows us to only estimate the time scale θ from spatial autocorrelations of the trajectories, but the exact physical interpretation of γ and k in the experiments is not possible. After every jump, the center position of the potential a is translated by an equal amount to maintain the particle inside the harmonic potential.

In our experiments, we observe a non-Gaussian to Gaussian transition over time (Fig. 3*C*). Such transition is likely caused by the underlying process of chloroplast motion, which is based on actin polymerization (21) in a highly dynamic and heterogeneous environment, resulting in temporal fluctuations of the active diffusion coefficient D. Therefore, we model the stochastic dynamics of the diffusion coefficient $D(t)$ by the square of an Ornstein–Uhlenbeck process (65, 66):

$$D(t) = Y(t)^2, \quad \dot{Y}(t) = -\frac{Y}{\tau} + \sigma\eta(t). \quad [2]$$

In the equation above, τ is a relaxation time scale, and σ is the noise amplitude of a Gaussian white noise $\eta(t)$. A similar formulation like in Eq. **2** has been used previously to describe active processes in cytoskeletal dynamics (67) and the transport of RNA (51) or colloidal beads on membranes (50). In the present context, Eq. **2** models fluctuations of the driving mechanism and environmental heterogeneity and leads to temporal correlations of the active diffusion coefficient. We support this assumption by observing that this "diffusing diffusivity" model (65) predicts an exponential distribution of diffusion coefficients (66) consistent with measurements of the diffusion coefficient of caged particles at times beyond 5 min (Fig. 3 *D*, *Inset*). This allows us to use the average active diffusion coefficient $\langle D \rangle = \sigma^2\tau = 8 \times 10^{-4}\ \frac{\mu m^2}{s}$ to estimate parameters for the model. Other parameters are extracted from particle trajectories and physiological parameters (*Materials and Methods*). A typical trajectory of this model displays diffusive dynamics with time-correlated variance and sudden jumps of discrete size (Fig. 5*B*). The resemblance to the experiments is also reflected in the van Hove function (Fig. 3*C*).

The discrete jumps can account for the exponential tails, while the non-Gaussian to Gaussian transition for increasing timescales and small displacements in the van Hove function can be well described by the diffusing diffusivity model.

Note that our model neglects the subdiffusive dynamics at small time scales (Fig. 3*A*) by construction (65, 66). Together with the damping parameter and the critical length scale, the effective diffusivity $D = \sigma^2\tau$ steers the caging dynamics, as observed in the MSD of the trajectories (Fig. 5*C* and *SI Appendix*, Fig. S3*A*). At a small noise amplitude σ, the system is strongly caged, as chloroplasts are drastically less probable to reach a high enough displacement to jump. If, however, σ is increased by 20 to 40%, the jumping dynamics are more pronounced, suggesting that chloroplasts are close to a critical point and can easily transition into a liquid-like state. In our model, this transition is, to a great extent, governed by the rate of jump events undertaken by the particle. We define the jump time distribution by construction as the first passage time distribution of an Ornstein–Uhlenbeck process at long timescales, at which the fluctuating diffusion coefficient approaches $D = \sigma^2\tau$. The first passage time distribution approaches a series of exponential functions (68), and the mean first passage time is controlled by a dimensionless quantity $x_c/\sqrt{D\theta}$ (69). This suggests that a similar transition is also possible when the critical length-scale x_c increases, while D is held constant (*SI Appendix*, Fig. S3), which has been observed in studies of plant cells with varying chloroplast numbers and areas (33). Hence, despite the simplified description of the cage effect and jumping dynamics, this model is sufficient to predict that not only the activity σ but also the critical size x_c can easily drive the system out of the caged dynamics.

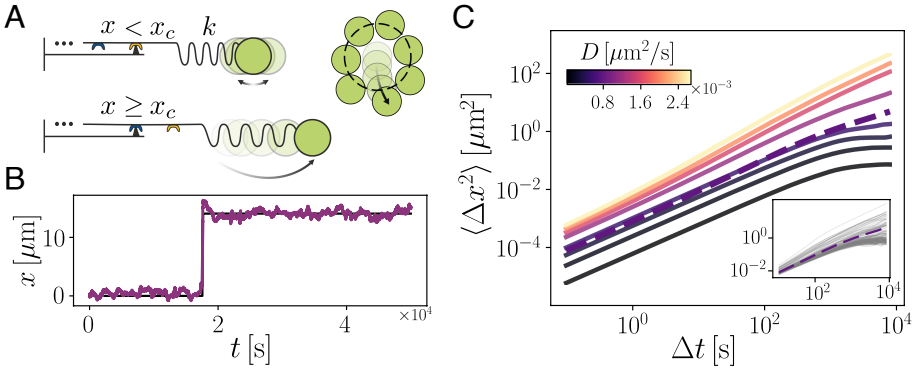

Fig. 5. Model based analysis suggests the vicinity of the chloroplast system to a dynamical transition. (*A*) Sketch of the mechanistic model. A Brownian particle is connected to a spring and a jump-element which undergoes sudden extension or compression if a critical displacement is reached. (*B*) Example trajectory shows sudden jumping events before being trapped again. (*C*) Ensemble-averaged MSD from low to large steady-state diffusion coefficients *D* shows a transition from trapped to free motion. Parameters obtained from our data suggest that the system is close to a transition towards unconfined motion. *Inset*: variability of trajectories shows dynamics ranging from caged to jumping motion, dashed line: ensemble average MSD with parameters from experiment.

Conclusion

Plants have developed multiple adaptation mechanisms to changing light conditions (28). One of these mechanisms is orchestrated via independent movements of disk-like chloroplasts toward or away from light. The motion of densely packed chloroplasts adapted to low-light conditions exhibits a striking similarity to the caged dynamics of supercooled liquids or colloidal suspensions close to glass transition. We observe actively driven organelles confined in a single layer at a high packing fraction. Intermittent coordinated motion of single or multiple chloroplasts leads to an exponentially tailed step-size distribution caused by the heterogeneous nature of the environment. Furthermore, we uncover dynamical features similar to systems close to the glass transition, such as dynamically heterogeneous regions, sudden chloroplast displacements, and even string-like coordinated movements. This renders chloroplasts a biological system exhibiting glassy behavior, while maintaining an unaltered disk-like shape, contrary to other biological active glasses like epithelial cell sheets (35–38, 41–43). A few other examples exist in which dense colloidal-like active particles play a physiological role, for example, in the context of active fluidization of statoliths, granular organelles in gravisensing plant cells (44), or the involvement of nuclear crowding in tissue stabilization (70).

To investigate the stability of the two-dimensional configuration of dim-light–adapted chloroplasts, we construct a one-dimensional model, whose parameters are obtained from experiments and physiological values. The statistics of this model are in agreement with our data. This indicates that burst-like chloroplast jumps could be triggered upon exceeding a threshold, similar to the cage length in glasses (52). By construction, the waiting times between the discrete jump events in this model are identical to the first-passage time of an Ornstein–Uhlenbeck process with diffusing diffusivity, which is approximately exponentially distributed for large-enough boundaries and times (68) (*SI Appendix*, Fig. S3*C*). This indicates that the underlying statistics of this model are similar to those of the continuous time random walk (CTRW) model proposed by Chaudhuri et al. (49, 55), which is used to describe a universal step-size distribution function in various systems close to the glass transition. However, this CTRW model needs the mean waiting time between jump events as a fit parameter, which is difficult to infer from limited data directly. Our model enabled us to convert a waiting time between jump events into a length scale x_c, which can be more easily extracted from data. Varying the model parameters suggests that chloroplasts operate at a metastable point and can easily perturb the monolayer structure by slight enhancements of their activity, which could explain the fast adaptation mechanism toward strong light, as observed in our experiments (Fig. 2). At later times in our experiments, we observe that chloroplasts break out of the monolayer and form three-dimensional (3D) clusters. The initiation of these dynamics requires the 2D phase to "fluidize" first, which is described by the model. The model also hints toward the important role of a cage effect inhibiting chloroplast photorelocation motion when the chloroplast size is changed, as has been observed before (33, 34).

We interpret our results as follows: Chloroplasts accumulate into a single layer in response to weak light in order to achieve a high surface coverage and therefore maximize photosynthetic efficiency (9). Since we know that chloroplasts avoid highly intense light (71), they must maintain the ability to undertake this avoidance motion efficiently without being hindered by other chloroplasts. Therefore, the ability to increase the activity and a sufficiently loose packing of chloroplasts are necessary. Our study shows that chloroplasts in dim-light conditions resemble a system close to the glass transition. Such a dynamical transition depends on the microscopic features of the organelles' propulsion mechanism as well as its cellular surrounding and can deviate from standard model glass forming systems. For example, chloroplasts can create protein bridges (18) and actin-cages (21); hence, the systems behavior may differ from purely repulsive, frictionless, or nonadhesive systems (72–76).

How chloroplasts spread on the periclinal cell walls as a result of an accumulation response under dim light remains a subject for further research since a direct observation of this process was not possible. Further studies on collective escape from this low-light–adapted state toward an avoidance configuration will shine light on the various dynamic phase transitions this system can undergo, which were also found in dense active matter systems (57, 77). Additionally, unveiling the exact interactive forces between the organelles and the impact of confinement due to the cell walls on the transitions between dark and light-adapted states remains a matter for further investigation.

Materials and Methods

Preparation and Imaging. *Elodea densa* was kept in an aquatic culture. Ambient light conditions were applied 1 h before image acquisition. For imaging, a low-light–adapted leaf was detached and placed between two glass slides. We study the lower cell layer of the two-layered leaf tissue (78), as these are more strongly involved in photosynthesis (79). The upper epidermal cell layer is important to enhance gas exchange due to reduced gas diffusion in water (80). Bright-field microscopy was performed with a `Nikon TI2` microscope using a halogen light source and a red-light 620 nm cut-on wavelength filter at low-light irradiance of approximately 1 W/m^2 in combination with a `Photometrics BSI Express` sCMOS camera with high quantum yield to enable imaging every 1 s with a 60× water-immersion objective (NA= 1.2) and pixel resolution of 0.11 μm/px. High light intensities for avoidance motion are achieved by removing the red-light filter and increasing the irradiance to approximately 600 W/m^2, approximately corresponding to the solar irradiance on a sunny day. The strong light shock was performed using the fluorescence lamp (`CoolLED pE-300`) at a peak wavelength of $\lambda = 466$ nm with an irradiance of approximately 10 kW/m^2 inducing rapid and irreversible depolymerization of actin and fixes of the sample. Confocal laser scanning microscopy was performed using a `Leica SP8`. The 638 nm excitation line and a broad band emission filter 650 to 750 nm were used to image chlorophyll autofluorescence. Z stacks were acquired over heights of 20 μm in 0.5 μm steps, while the z-resolution is 860 nm with an 60× oil immersion objective (NA = 1.4).

Image Processing. Image time series were background-subtracted using a difference-of-Gaussian method with variances $\sigma_1 = 2$ px and $\sigma_2 = 37$ px and subsequently inverted (*SI Appendix*, Fig. S4). The resulting image shows white circular spots, reminiscent of nuclei training data for the StarDist versatile model (81). Using this pretrained StarDist network, we segmented the images and detect center-of-mass positions of the particles. The segmented objects were analyzed for their area and aspect ratio. Small objects of an area of 250 px, corresponding to an equivalent diameter of less than 1.78 μm, were removed. Additionally, elongated objects with aspect ratios of above 3.5 or below 0.3 were excluded to avoid misdetections of cell walls. We hand-segmented the surrounding cell wall to discriminate chloroplasts in different cells (*SI Appendix*, Fig. S1*B*). Histograms for the particle diameters and aspect ratios, as well as the packing fraction, were calculated based on hand-segmented chloroplasts to avoid detection biases and smaller mistakes in the StarDist-based segmentation. The average packing fraction was calculated by the sum of all areas of segmented chloroplast divided by the area of the segmented cells.

Trajectory Analysis. The center-of-mass positions of all segmented chloroplasts were linked to trajectories using a linear assignment problem solver trackpy (82). Spurious trajectories of a duration smaller than 400 s were not considered in the analysis. Trajectories were classified as fast when their maximal displacement lies above the mean particle size (dashed line in Fig. 4*C* and *SI Appendix*, Fig. S1*G*)(54, 56) and whose maximal velocity lies above 0.1 μm/s. Particle velocities were calculated with the first derivative of the third-order Savitzky–Golay filtered data, with a kernel length of 11 s. The self-part of the van Hove function and the mean squared displacements were calculated with trackpy (82), while the MSD scaling exponents α were extracted using a local fitting scheme (83) between $\Delta t = 10 - 100$ s. As we track the center of mass of the segmented particles, we have two contributions to the error of the tracking algorithm: one from the limited pixel-size of $\sigma_{px} = 0.11\,\mu$m and area fluctuations of the mass. As the mask can differ from image to image, we take the area fluctuations as a proxy to estimate a detection error: $\sigma \approx \sigma_{px}\sqrt{\sigma_A/\langle A\rangle} \approx 0.07\,\mu$m, with the mean $\langle A\rangle$ and the SD σ_A of the areas obtained by temporal and ensemble averaging over all trajectories.

Simulations. Our model (Eqs. **1** and **2**) was integrated using a stochastic Euler–Maruyama scheme with 10^6 time steps of duration $dt = 0.1$ s. Simulation parameters were retrieved from trajectories. We choose the $1/e$ decay of the positional autocorrelation function (*SI Appendix*, Fig. S1*I*) to estimate the harmonic relaxation time $\theta = 1{,}063$ s. Although the function does not follow an exponential decay, it gives a reasonable estimate for the correlation time. Additionally, we estimated the noise amplitude σ of the diffusing diffusivity from the measurements of the long-time diffusion coefficients of the system as $D = \sigma^2\tau$. Here, we set the correlation time $\tau = 90$ s, which is well within the range of actin turnover times (84). The jump velocity $v \approx 0.6\,\mu$m/s was estimated from the average maximal velocity of jumping chloroplasts. The critical length scale $x_c = 2.3\,\mu$m is the point at which the van Hove function transitions to an exponential (Fig. 3*C*). This critical length scale is close to the average particle radius (*SI Appendix*, Fig. S1*G*). For parameter sweeps, x_c^{-1} and σ were changed from 20% to 180% of their experimental value, and simulations were repeated 200 times for each parameter. Simulation data were analyzed exactly the same as trajectories. The continuous time random walk model (Fig. 3*C*, dashed line) was implemented as outlined in (46) with parameters $\tau_1 = 3{,}000$ s, $\tau_2 = 100$ s, $d = 0.6\,\mu$m, $l = 1.2\,\mu$m.

Data, Materials, and Software Availability. csv files of trajectories and raw microscopy data have been deposited in Zenodo 10.5281/zenodo/6517229.

ACKNOWLEDGMENTS. We are grateful to Federico Caporaletti, Vincent Debets, Liesbeth Janssen, Ludovic Berthier, and Carola Seyfert for invaluable discussions and assistance. N.S. thanks Robert Haase for insightful discussions on object tracking at an early stage of the project.

1. C. W. Whippo, R. P. Hangarter, The "sensational" power of movement in plants: A Darwinian system for studying the evolution of behavior. *Am. J. Bot.* **96**, 2115–2127 (2009).
2. A. D. Carpenter, Embodied intelligent (?) souls: Plants in plato's timaeus. *Phronesis* **55**, 281–303 (2010).
3. C. Darwin, F. Darwin *et al.*, *The Power of Movement in Plants* (D. Appleton and Company, 1883).
4. Y. Forterre, Slow, fast and furious: Understanding the physics of plant movements. *J. Exp. Bot.* **64**, 4745–4760 (2013).
5. D. E. Moulton, H. Oliveri, A. Goriely, Multiscale integration of environmental stimuli in plant tropism produces complex behaviors. *Proc. Natl. Acad. Sci. U.S.A.* **117**, 32226–32237 (2020).
6. E. Liscum *et al.*, Phototropism: Growing towards an understanding of plant movement. *Plant Cell* **26**, 38–55 (2014).
7. M. Kasahara *et al.*, Chlomplast avoidance movement reduces photodamage in plants. *Nature* **420**, 829–832 (2002).
8. M. Wada, Chloroplast movement. *Plant Sci.* **210**, 177–182 (2013).
9. E. Gotoh *et al.*, Chloroplast accumulation response enhances leaf photosynthesis and plant biomass production. *Plant Physiol.* **178**, 1358–1369 (2018).
10. J. A. Von Böhm, Beiträge zur näheren Kenntniss des Chlorophylls. *S.B. Math-nat. Kl. Akad. Wiss.* **22**, 479–512 (1856).
11. B. Frank, Ueber lichtwärts sich bewegende Chlorophyllkörner. *Bot. Ztg.* **29**, 225–232 (1871).
12. G. Senn *et al.*, *Gestalts-und Lageveranderung der Pflanzen-Chromatophoren* (W. Engelmann, 1908).
13. W. Haupt, Light-mediated movement of chloroplasts. *Ann. Rev. Plant Physiol.* **33**, 205–233 (1982).
14. H. Tsuboi, H. Yamashita, M. Wada, Chloroplasts do not have a polarity for light-induced accumulation movement. *J. Plant Res.* **122**, 131–140 (2009).
15. H. Tsuboi, M. Wada, Chloroplasts can move in any direction to avoid strong light. *J. Plant Res.* **124**, 201–210 (2011).
16. T. Sakai *et al.*, Arabidopsis nph1 and npl1: Blue light receptors that mediate both phototropism and chloroplast relocation. *Proc. Natl. Acad. Sci. U.S.A.* **98**, 6969–6974 (2001).
17. N. Suetsugu, M. Wada, Signalling mechanism of phototropin-mediated chloroplast movement in *Arabidopsis*. *J. Plant Biochem. Biotechnol.* **29**, 580–589 (2020).
18. S.-G. Kong *et al.*, Chloroplast unusual positioning 1 is a new type of actin nucleation factor in plants. bioRxiv [Preprint] (2020). https://www.biorxiv.org/content/early/2020/01/15/2020.01.14.905984. Accessed 4 February 2022.
19. K. Oikawa *et al.*, Chloroplast unusual positioning1 is essential for proper chloroplast positioning. *Plant Cell* **15**, 2805–2815 (2003).
20. K. Oikawa *et al.*, Chloroplast outer envelope protein Chup1 is essential for chloroplast anchorage to the plasma membrane and chloroplast movement. *Plant Physiol.* **148**, 829–842 (2008).
21. A. Kadota *et al.*, Short actin-based mechanism for light-directed chloroplast movement in *Arabidopsis*. *Proc. Natl. Acad. Sci. U.S.A.* **106**, 13106–13111 (2009).
22. S. G. Kong, Y. Arai, N. Suetsugu, T. Yanagida, M. Wada, Rapid severing and motility of chloroplast-actin filaments are required for the chloroplast avoidance response in *Arabidopsis*. *Plant Cell* **25**, 572–590 (2013).
23. C. W. Whippo *et al.*, THRUMIN1 is a light-regulated actin-bundling protein involved in chloroplast motility. *Curr. Biol.* **21**, 59–64 (2011).
24. M. Wada, S. G. Kong, Actin-mediated movement of chloroplasts. *J. Cell Sci.* **131** (2018).
25. T. Kagawa, M. Wada, Velocity of chloroplast avoidance movement is fluence rate dependent. *Photochem. Photobiol. Sci.* **3**, 592–595 (2004).
26. S. Takahashi, M. R. Badger, Photoprotection in plants: A new light on photosystem II damage. *Trends Plant Sci.* **16**, 53–60 (2011).
27. Y. I. Park, W. S. Chow, J. M. Andersen, Chloroplast movement in the shade plant tradescantia albiflora helps protect photosystem II against light stress. *Plant Physiol.* **111**, 867–875 (1996).
28. Z. Li, S. Wakao, B. B. Fischer, K. K. Niyogi, Sensing and responding to excess light. *Ann. Rev. Plant Biol.* **60**, 239–260 (2009).
29. T. Kagawa, M. Wada, Phytochrome- And blue-light-absorbing pigment-mediated directional movement of chloroplasts in dark-adapted prothallial cells of fern Adiantum as analyzed by microbeam irradiation. *Planta* **198**, 488–493 (1996).
30. J. Zurzycki, The dependence of photosynthesis on the arrangement of chloroplasts. *Experientia* **11**, 263–263 (1955).
31. S. I. Honda, T. Hongladarom-Honda, P. Kwanyuen, S. G. Wildman, Interpretations on chloroplast reproduction derived from correlations between cells and chloroplasts. *Planta* **97**, 1–15 (1971).
32. J. R. Ellis, R. M. Leech, Cell size and chloroplast size in relation to chloroplast replication in light-grown wheat leaves. *Planta* **165**, 120–125 (1985).
33. M. Königer, J. A. Delamaide, E. D. Marlow, G. C. Harris, Arabidopsis thaliana leaves with altered chloroplast numbers and chloroplast movement exhibit impaired adjustments to both low and high light. *J. Exp. Bot.* **59**, 2285–2297 (2008).
34. D. C. McCain, Chloroplast movement can be impeded by crowding. *Plant Sci.* **135**, 219–225break (1998).
35. T. E. Angelini *et al.*, Glass-like dynamics of collective cell migration. *Proc. Natl. Acad. Sci. U.S.A.* **108**, 4714–4719 (2011).
36. S. Garcia *et al.*, Physics of active jamming during collective cellular motion in a monolayer. *Proc. Natl. Acad. Sci. U.S.A.* **112**, 15314–15319 (2015).
37. M. Sadati, N. T. Qazvini, R. Krishnan, C. Y. Park, J. J. Fredberg, Collective migration and cell jamming. *Differentiation* **86**, 121–125 (2013).
38. L. Atia *et al.*, Geometric constraints during epithelial jamming. *Nat. Phys.* **14**, 613–620 (2018).
39. D. Bi, X. Yang, M. C. Marchetti, M. Lisa Manning, Motility-driven glass and jamming transitions in biological tissues. *Phys. Rev. X* **6**, 1–13 (2016).
40. S. Kim, M. Pochitaloff, G. A. Stooke-Vaughan, O. Campàs, Embryonic tissues as active foams. *Nat. Phys.* **17**, 859–866 (2021).
41. A. Mongera *et al.*, A fluid-to-solid jamming transition underlies vertebrate body axis elongation. *Nature* **561**, 401–405 (2018).
42. J. A. Park *et al.*, Unjamming and cell shape in the asthmatic airway epithelium. *Nat. Mater.* **14**, 1040–1048 (2015).
43. L. Oswald, S. Grosser, D. M. Smith, J. A. Käs, Jamming transitions in cancer. *J. Phys. D. Appl. Phys.* **50**, 483001 (2017).
44. A. Bérut *et al.*, Gravisensors in plant cells behave like an active granular liquid. *Proc. Natl. Acad. Sci. U.S.A.* **115**, 5123–5128 (2018).
45. B. R. Parry *et al.*, The bacterial cytoplasm has glass-like properties and is fluidized by metabolic activity. *Cell* **156**, 183–194 (2014).
46. C. Åberg, B. Poolman, Glass-like characteristics of intracellular motion in human cells. *Biophys. J.* **120**, 2355–2366 (2021).
47. L. M.C. Janssen, Active glasses. *J. Phys. Condens. Matter* **31**, 503002 (2019).
48. Y. Sakai, S. Takagi, Roles of actin cytoskeleton for regulation of chloroplast anchoring. *Plant Signal. Behav.* **12**, e1370163 (2017).
49. P. Chaudhuri, L. Berthier, W. Kob, Universal nature of particle displacements close to glass and jamming transitions. *Phys. Rev. Lett.* **99**, 2–5 (2007).
50. B. Wang, S. M. Anthony, C. B. Sung, S. Granick, Anomalous yet Brownian. *Proc. Natl. Acad. Sci. U.S.A.* **106**, 15160–15164 (2009).
51. T. J. Lampo, S. Stylianidou, M. P. Backlund, P. A. Wiggins, A. J. Spakowitz, Cytoplasmic RNA-protein particles exhibit non-Gaussian subdiffusive behavior. *Biophys. J.* **112**, 532–542 (2017).
52. V. E. Debets, X. M. de Wit, L. M. C. Janssen, Cage length controls the non-monotonic dynamics of active glassy matter. *Phys. Rev. Lett.* **127**, 278002 (2021).
53. M. D. Ediger, Spatially heterogeneous dynamics in supercooled liquids. *Annu. Rev. Phys. Chem.* **51**, 99–128 (2000).
54. W. K. Kegel, A. van Blaaderen, Direct observation of dynamical heterogeneities in colloidal hard-sphere suspensions. *Science* **287**, 290–293 (2000).

55. P. Chaudhuri, Y. Gao, L. Berthier, M. Kilfoil, W. Kob, A random walk description of the heterogeneous glassy dynamics of attracting colloids. *J. Phys. Condens. Matter* **20**, 244126 (2008).
56. W. Kob, C. Donati, S. J. Plimpton, P. H. Poole, S. C. Glotzer, Dynamical heterogeneities in a supercooled Lennard-Jones liquid. *Phys. Rev. Lett.* **79**, 2827–2830 (1997).
57. R. Mandal, P. J. Bhuyan, P. Chaudhuri, C. Dasgupta, M. Rao, Extreme active matter at high densities. *Nat. Commun.* **11**, 1–8 (2020).
58. G. Marty, O. Dauchot, Subdiffusion and cage effect in a sheared granular material. *Phys. Rev. Lett.* **94**, 1–4 (2005).
59. M. T. Cicerone, Q. Zhong, M. Tyagi, Picosecond dynamic heterogeneity, hopping, and johari-goldstein relaxation in glass-forming liquids. *Phys. Rev. Lett.* **113**, 8–12 (2014).
60. F. Caporaletti *et al*., Experimental evidence of mosaic structure in strongly supercooled molecular liquids. *Nat. Commun.* **12**, 6–12 (2021).
61. C. Donati *et al*., Stringlike cooperative motion in a supercooled liquid. *Phys. Rev. Lett.* **80**, 2338–2341 (1998).
62. A. S. Keys, A. R. Abate, S. C. Glotzer, D. J. Durian, Measurement of growing dynamical length scales and prediction of the jamming transition in a granular material. *Nat. Phys.* **3**, 260–264 (2007).
63. B. Doliwa, A. Heuer, C. effect, local anisotropies, and dynamic heterogeneities at the glass transition: A computer study of hard spheres. *Phys. Rev. Lett.* **80**, 4915–4918 (1998).
64. E. R. Weeks, D. A. Weitz, Properties of cage rearrangements observed near the colloidal glass transition. *Phys. Rev. Lett.* **89**, 1–4 (2002).
65. M. V. Chubynsky, G. W. Slater, Diffusing diffusivity: A model for anomalous, yet Brownian, diffusion. *Phys. Rev. Lett.* **113**, 1–5 (2014).
66. A. V. Chechkin, F. Seno, R. Metzler, I. M. Sokolov, Brownian yet non-Gaussian diffusion: From superstatistics to subordination of diffusing diffusivities. *Phys. Rev. X* **7**, 1–20 (2017). 10.1103/PhysRevX.7.021002.
67. T. Toyota, D. A. Head, C. F. Schmidt, D. Mizuno. Non-Gaussian athermal fluctuations in active gels. *Soft Matter* **7**, 3234–3239 (2011). 10.1039/c0sm00925c.
68. L. M. Ricciardi, S. Sato, First-passage-time density and moments of the Ornstein-Uhlenbeck process. *J. Appl. Probab.* **25**, 43–57 (1988). 10.2307/3214232.
69. A. G. Nobile, L. M. Ricciardi, L. Sacerdote, Exponential trends of Ornstein-Uhlenbeck first-passage-time densities. *J. Appl. Probab.* **22**, 360–369 (1985). http://www.jstor.org/stable/3213779.
70. S. Kim, R. Amini, O. Campàs. A nuclear jamming transition in vertebrate organogenesis. bioRxiv, 2022. 10.1101/2022.07.31.502244. Accessed 3 August 2022.
71. M. Wada, T. Kagawa, Y. Sato. Chloroplast movement. *Ann. Rev. Plant Biol.* **54**, 455–468 (2003). 10.1146/annurev.arplant.54.031902.135023.
72. E. Zaccarelli, W. C. K. Poon. Colloidal glasses and gels: The interplay of bonding and caging. *Proc. Natl. Acad. Sci. U.S.A.* **106**, 15203–15208 (2009). 10.1073/pnas.0902294106.
73. J. A. Richards, B. M. Guy, E. Blanco, M. Hermes, G. Poy, W. C. K. Poon. The role of friction in the yielding of adhesive non-Brownian suspensions. *J. Rheol.* **64**, 405–412 (2020). 10.1122/1.5132395.
74. D. Bonn, M. M. Denn, L. Berthier, T. Divoux, S. Manneville, Yield stress materials in soft condensed matter. *Rev. Mod. Phys.* **89**, 035005 (2017).
75. L. Berthier, G. Biroli. Theoretical perspective on the glass transition and amorphous materials. *Rev. Mod. Phys.* **83**, 587–645 (2011). 10.1103/RevModPhys.83.587.
76. P. Charbonneau, J. Kurchan, G. Parisi, P. Urbani, F. Zamponi, Glass and jamming transitions: From exact results to finite-dimensional descriptions. *Ann. Rev. Condens. Matter Phys.* **8**, 265–288 (2017). 10.1146/annurev-conmatphys-031016-025334.
77. Y. K. Keta, R. L. Jack, L. Berthier. Disordered collective motion in dense assemblies of persistent particles. *Phys. Rev. Lett.* **129**, 48002 (2022). 10.1103/PhysRevLett.129.048002. http://arxiv.org/abs/2201.04902.
78. N. Rascio, P. Mariani, E. Tommasini, M. Bodner, W. Larcher. Photosynthetic strategies in leaves and stems of *Egeria densa*. *Planta* **185**, 297–303 (1991). 10.1007/BF00201047.
79. E. Maai, K. Nishimura, R. Takisawa, T. Nakazaki, Light stress-induced chloroplast movement and midday depression of photosynthesis in sorghum leaves. *Plant Production Sci.* **23**, 172–181 (2020). 10.1080/1343943X.2019.1673666.
80. O. Pedersen, T. D. Colmer, K. Sand-Jensen, Underwater photosynthesis of submerged plants - recent advances and methods. *Front. Plant Sci.* **4**, 1–19 (2013). 10.3389/fpls.2013.00140.
81. M. Weigert, U. Schmidt, R. Haase, K. Sugawara, G. Myers. "Star-convex polyhedra for 3D object detection and segmentation in microscopy" in *Proceedings - 2020 IEEE Winter Conference on Applications of C. Vision, WACV 2020* (2020), pp. 3655–3662. 10.1109/WACV45572.2020.9093435.
82. D. B. Allan, T. Caswell, N. C. Keim, C. M. van der Wel, R. W. Verweij, Soft-matter/trackpy: Trackpy v0.5.0. Zenodo, April 2021. 10.5281/zenodo.4682814.
83. T. Maier, T. Haraszti, Python algorithms in particle tracking microrheology. *Chem. Central J.* **6**, 1–9 (2012). 10.1186/1752-153X-6-144.
84. L. Blanchoin, R. Boujemaa-Paterski, J. L. Henty, P. Khurana, C. J. Staiger, Actin dynamics in plant cells: A team effort from multiple proteins orchestrates this very fast-paced game. *Curr. Opin. Plant Biol.* **13**, 714–723 (2010). 10.1016/j.pbi.2010.09.013.